Research on Engineering Structures & Materials
journal homepage: http://jresm.org
MIM Research Group

Research Article

Evaluation of nano sized Mg@BTC metal organic framework as a drug carrier: A long term experimental and predictive theoretical study

Güliz Akyüz[1,a], Aykut Elmas[*1,b], Müberra Andaç[1,2,c], Ömer Andaç[1,2,d]

[1]*Department of Nanoscience and Nanotechnology, Ondokuz Mayıs University, Samsun, Turkey*
[2]*Department of Chemistry, Ondokuz Mayıs University, Samsun, Turkey*

Article Info

Article history:
Received 13 Jun 2020
Revised 25 Oct 2020
Accepted 27 Oct 2020

Keywords:

Long term release;
Nano sized Mg@BTC;
Drug carrier;
Model fit tests;
Slow release

Abstract

Metal Organic Frameworks (MOFs) have found wide applications as a drug carrier in nanotherapeutics because of adjustable pore-sizes, controllable structural properties, large surface area and high pore volume. In this work, nanosized Mg@BTC is synthesized by electrochemical method and used as a new drug carrier for ibuprofen. The ibuprofen (IB) is loaded to the Mg@BTC 1:1 ratio with the amount of %99.8. The release of ibuprofen from nanocarrier has been observed experimentally for long term. After 100.5 hours, the release ratio yields 36 %. The ibuprofen has been tested at 40 ± 0.5 °C. System showed a rapid release after 100 hours, the release ratio yields 72.29 %. The release profile of IB loaded Mg@BTC is tested by using model depended mathematical models to get observation and prediction of the release. Zero Order Model, First Order Model, Higuchi Model, Peppas Model and Hixon Model functions are fitted to the release profiles. Watson's U Squared Method is used to test the fit strength of the models. Observation from the release profiles, it is seemed Peppas Model yields the best results. Also, thermodynamic analysis has been studied.

1. Introduction

Porous materials with high surface area have always attracted attention for nanotechnological applications. The various molecular structures, properties and promising applications are some of the main reasons of this attention. Metal organic frameworks (MOFs) can be considered as one of the most popular porous materials. As a short description, MOFs are self-assembly, branched and high porosity crystalline polymers which possess metal ions with organic linkers. Examples of some common linkers are oxalic acid, terephthalic acid, trimesic acid, adamantane-1,3,5,7-tetracarboxylic acid, fumaric acid, 4,5-imidazoledicarboxylicacid, 1,4-butanedicarboxylic acid, 4,6-dihydroxy benzene-1,2,5-trisulfonic acid, biphenyl-4,4-dicarboxylic acid, 2,5-dihydroxyterephthalic acid, 6,6-dichloro-4,4-di(pyridin-4-yl)-1,1-binaphthyl-2,2-diol, 6-naphthalenedicarboxylic acid and 1,3,5-benzenetribenzoic acid respectively [1].

Besides, various combinations of metals and ligands or method types can be used for obtaining different MOFs. Some of the synthesis methods are hydro-thermal method, microwave and ultrasonic methods, electrochemical synthesis, mechanochemical synthesis, diffusion method, solvent evaporation and ionothermal synthesis respectively [1-3].

*Corresponding author: aykutdiamond@gmail.com
[a]orcid.org/0000-0002-3522-9716; [b]orcid.org/0000-0002-7721-4088; [c] orcid.org/0000-0001-7262-9762; [d] orcid.org/0000-0003-3641-9690
DOI: http://dx.doi.org/10.17515/resm2020.199na0613

MOF's non-toxic activity is related to synthesis method and chemicals which are used in the process. Obtaining biocompatible MOFs with green synthesis methods which support to eliminate the use of toxic chemicals is possible. Electrochemical and sonochemical methods are developed for this purpose [3, 4].

MOFs should have minimal toxic effects when they enter the body system. Some metals are highly toxic like chromium. But some of them present in the body with less toxicity and large quantities. Such as; iron, calcium, copper, zinc, manganese. Their oral lethal dose is below 50 (LD50) in the body [1].

Metal organic frameworks have been applied on several fields [5-10]. Major applications of MOFs are light emitting devices [11, 12] and sensors [3, 11], gas storage [13, 14], magnets [15, 16], catalysts [17, 18] and drug delivery [1-3, 19-21].

In recent years, MOF based therapies have started to attract attention. Many strategies have developed in order to increase the effect of conventional therapeutics. Many drawbacks of small molecule drugs can be controlled by the use of new developments of drug delivery. MOFs have a very important role in the controlled drug release due to their pore size, shape, structure and chemical properties, adjustable structure, a large surface area and large pore sizes. Thus, the encapsulation of different types of drugs have been studied.

Vasconcelos et al. [22] prepared Zn@BDC and doxorubicin loaded into structure (DOX@Zn@BDC). The drug delivery system showed slower release and studies of cytotoxicity showed good results for the system developed with antineoplastic doxorubicin. Abbasia and Rizvandia [2] investigated the release properties of rifampicin from Cu@BTC nanoparticles. Furthermore, Lestari et al. [3] studied on Zn@BTC and investigated its ability in loading and slow release of ibuprofen. Ibuprofen is a propionic acid derivative and a nonsteroid anti-inflammatory drug. It is used for anti-inflammatory, antipyretic, and analgesic effects. It has been used in the treatment of osteoarthritis, rheumatoid arthritis, gout, mild and moderate pains [23, 24].

In this study, nano sized Mg@BTC were synthesized and first time used as a drug carrier. For synthesis and functionalized of Mg@BTC, electrochemical method was used which supports to eliminate the use of toxic chemicals. Besides, evaluation of Mg@BTC for controlled release of ibuprofen was observed for long term up to 100 hours at different temperature conditions contrary to many studies.

Also, a predictive research has taken place in the consideration of mathematical modeling of drug release profile. The reason of the testing the system with models is to predict the release behavior of the drug and generate more effective experiments for avoiding waste of time and money. Mathematical models can represent different types of kinetics of drug release profile depending on the system. In this work, five models are chosen. Zero Order Model and First Order Model are derived from the reaction kinetics of the chemistry [25]. They are very popular in the field. In addition to these models, the Higuchi Model [26], Peppas Model [27], and Hixon Model [28] are also chosen to for the testing because of their strength between the all other models. All of the three models are used for testing the results of long term drug release profile of the MOF both which described below.

After the fitting procedure, numerical comparison of the models is generated. It is chosen the Watson's U-Squared test [29] for the convenience of the system and the results are compared vie the computer software.

Also, thermodynamic parameters has been generated by using Arrhenius equation, Erying equation and Gibbs free energy equation [30].

2. Experimental

2.1. Materials and methods

Methanol (99%), NaCl (99%), KCl (99%), Na_2HPO_4 (99%), KH_2PO_4 (99%), NaOH, HCl, tween 20, benzene-1,3,5-tri-carboxylic acid (H_3BTC, 99%), n-hexane (99%), tetrabutylammoniumtetrafloroborate (TBATFB, 99%) were purchased from Sigma Aldrich. Na-ibuprofen (99%) was provided commercially by Adeka. The phosphate buffer saline (PBS) solution was prepared according to procedure [31]. Magnesium metal plates were used as the electrodes. The synthesized [Mg@BTC] and ibu@[Mg@BTC] were characterized using X-ray diffraction spectroscopy (XRD) (Rigaku Smart lab). Concentration of loaded and released ibuprofen was analyzed using UV-Vis spectroscopy (Thermo scientific evolution 220, PCCU1). The FTIR spectra (PerkinElmer, Spectrum two, USA) of the samples were recorded with an infrared spectrometer to characterize the MOF and, it was recorded in a range of 400–4000 cm^{-1} using spectrometer. The surface morphology and particles sizes of the samples were carried out using high resolution scanning electron microscopy (SEM) (JEOL-JSM-7001F). The energy dispersive spectrometry (EDS) analysis as also studied. Atomic force microscope (AFM) (NT-MDT NEXT, Russia) was used to determine the morphology of MOF. All measurements were performed at room temperature.

2.2. Electro-chemical synthesis of [Mg@BTC]

Electro-chemical synthesis of [Mg@BTC] was studied according to the procedure previously described [3]. Two plates of magnesium metal were used as electrodes and activated by polishing using sandpaper. Plates initial masses were respectively 0,6969 g and 0,6782 g. The ligand H_3BTC (5.25 g) and the electrolyte tetrabutylammoniumtetrafluoro-borate (TBATFB) (4.11 g) were dissolved in the methanol (250 mL) and stirred for 15 min. The magnesium plates were placed inside the electrochemical cell. Electrolysis was verified using an ambient temperature under a voltage of 3 V 9.5 mA for 4 hours. The white precipitate that resulted from the reaction was washed three times with methanol and dried at room temperature for 24 h and further activated at 120 °C for 48 hours.

2.3. In vitro loading ibuprofen into [Mg@BTC] and release study

The mass variation of loaded ibuprofen into [Mg@BTC] are in ratio 1:1 (g/g). Ibuprofen (0.1525 g) was dissolved in 10 mL of n-hexane, then [Mg@BTC] (0.1525 g) was added and stirred for 72 h at an ambient temperature. The suspension was then centrifuged, washed with n-hexane and the remaining filtrate were analyzed using UV-Vis spectroscopy to determine the rest of the unloaded ibuprofen. The precipitate was dried at room temperature for 24 h and then called as ibu@[Mg@BTC] and placed in 25 mL of phosphate buffer saline (PBS) containing tween 20 (0.5% v/v) at physiological pH, temperature of 36 ± 0.5 °C and stirred constantly for time intervals 0.25, 0.5, 1, 1.5, 2.25, 3, 4, 4, 5, 7, 9, 24, 30, 48, 54, 72, 100.5 h. 2.5 mL of solution from each buffer was harvested overtime with subsequent replacement of equal volume of fresh buffer at the different time interval.

Moreover, release study was tested by high temperature condition (40 ± 0.5 °C). The same experimental conditions were maintained with temperature of 36 ± 0.5 °C and the temperature of the experimental system was set at 40 ± 0.5 °C. Equal volume of samples were collected for different time intervals 0.25, 0.5, 1, 1.5, 2.25, 3, 4, 4, 5, 7, 9, 24, 30, 48, 54, 72, 100.5 h. The release of the ibuprofen was then quantified by measuring its absorbance using absorption spectroscopy at 228 nm and the concentration of the released ibuprofen calculated with the aid of a standard curve.

For the all fitting procedure of the models, graphical representations and thermodynamic calculations, The Wolfram Mathematica software is used. Also, Watson's U-Squared method is chosen for the quantitative strength test of the fit functions [29]. The model functions are defined by the user for suitable data set. But for the graphical representation, model fitting and testing method, build-in functions are preferred to use because of the effective user interference.

3. Result and Discussion

FTIR spectroscopy was carried out to the identification of structure analysis of Mg@BTC. The spectra of the synthesized Mg@BTC powder was recorded. The spectrum of the powder is illustrated in Fig. 1. The bond formation between the tricarboxylic acid and the magnesium metal ions were observed from the significant shift of carbonyl (C=O) peak from carboxylate at 1700-1400 cm^{-1}. This shift corresponded to the formation of coordination bonding in Mg@BTC as shown in Fig. 1. Besides, absorption peaks in the 1100-900 cm^{-1} band was observed due to the vibration of the C-O bond in the carboxylate group [4, 32]. Since there is no broad peak centered at around 3300 cm^{-1}, Mg@BTC does not contain water

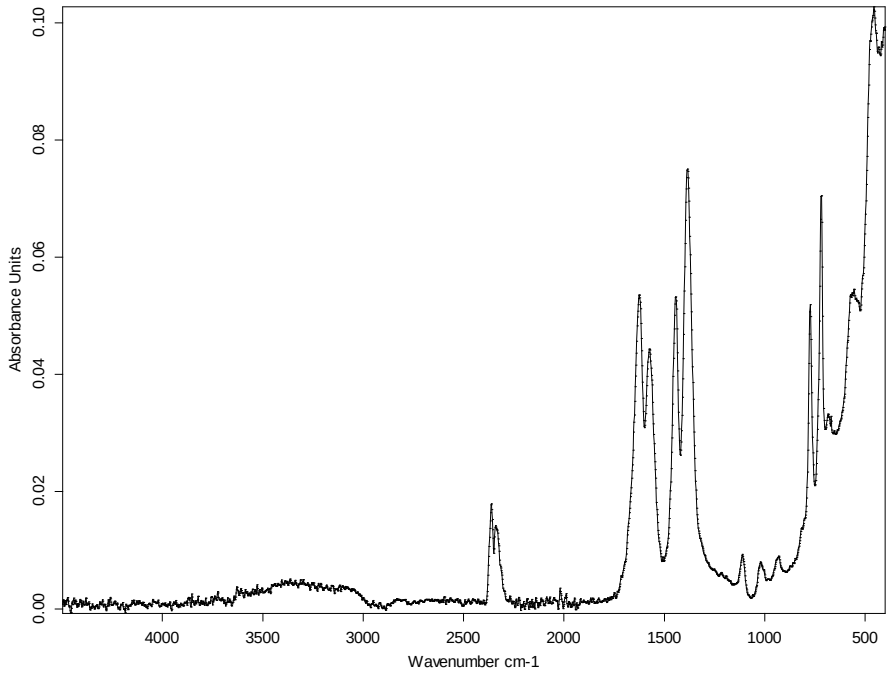

Fig. 1 FTR spectra of Mg@BTC.

The thermal decomposition of Mg@BTC was shown in Fig. 2. In general, three steps of mass loss process were observed [4]. In the first stage, the loss of water molecules at temperatures up to 20-80 °C. Approximately 3% mass loss was observed. 16.43% mass loss was detected after the releasing of the methanol from the structure at temperatures up to 80-550 °C. Besides, 50.57 % mass loss was observed at temperatures up to 550 °C-655 °C. The final mass of Mg@BTC was 29 % at 888 °C.

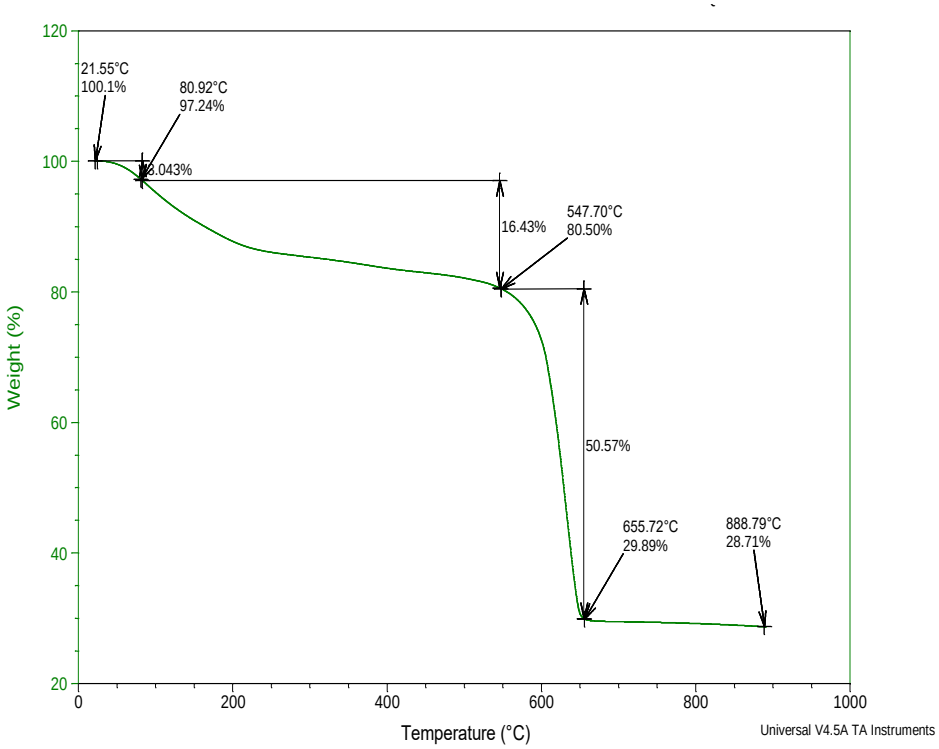

Fig. 2. TGA curve of Mg@BTC.

The crystal structures of all the synthesized Mg@BTC were confirmed by powder X-ray diffraction (XRD) using a Rigaku Smart lab. Diffraction patterns were collected at a scan rate of 2^{o} min^{-1} at 0.02^{o} steps from 10 to 80^{o} two theta.

In our study, solvent-free 3D Mg@BTC was obtained owing to the synthesis in methanol. However, indexing could not be performed due to the low crystallinity of the structure. The powder XRD diffraction patterns were given in Fig. 3. The X-ray diffraction pattern of the Mg@BTC is similar to that reported previously study of Bella et al. [33].

SEM images of nano sized Mg@BTC are given in Fig 4, Fig 5, Fig. 6 and Fig. 7. Powder samples are attached to the carbon band. When the morphology of Mg@BTC is examined, Mg@BTC particles are filamentous in shape and their sizes vary in the range of 30-90 nm. SEM images in Fig 4, Fig 5, Fig. 6 and Fig. 7 are in good agreement with EDS results of Mg@BTC which are shown in Fig. 8 and Fig. 9. The chemical composition of Mg@BTC was investigated via EDS, and EDS mapping analysis and spectrum are shown in Fig. 8 and Fig. 9. EDS mapping analysis and spectrum of Mg@BTC confirms the nanoparticles in which Mg, C, and O are present.

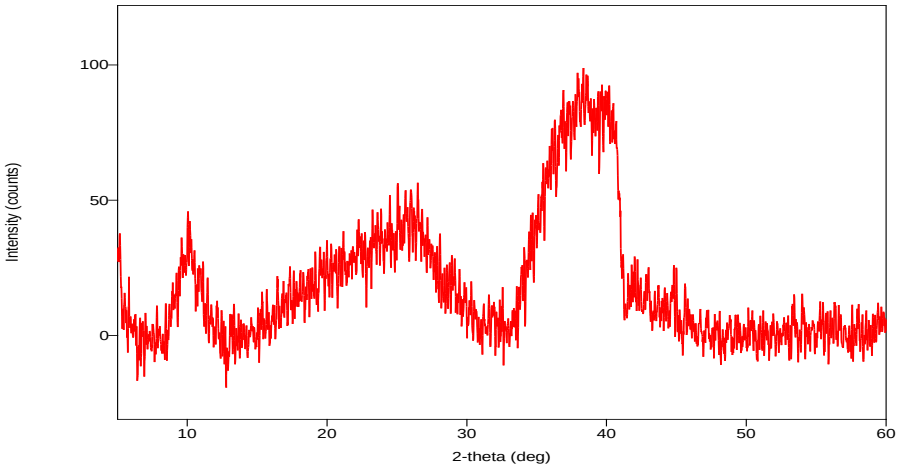

Fig. 3 XRD diffraction pattern of nano sized Mg@BTC

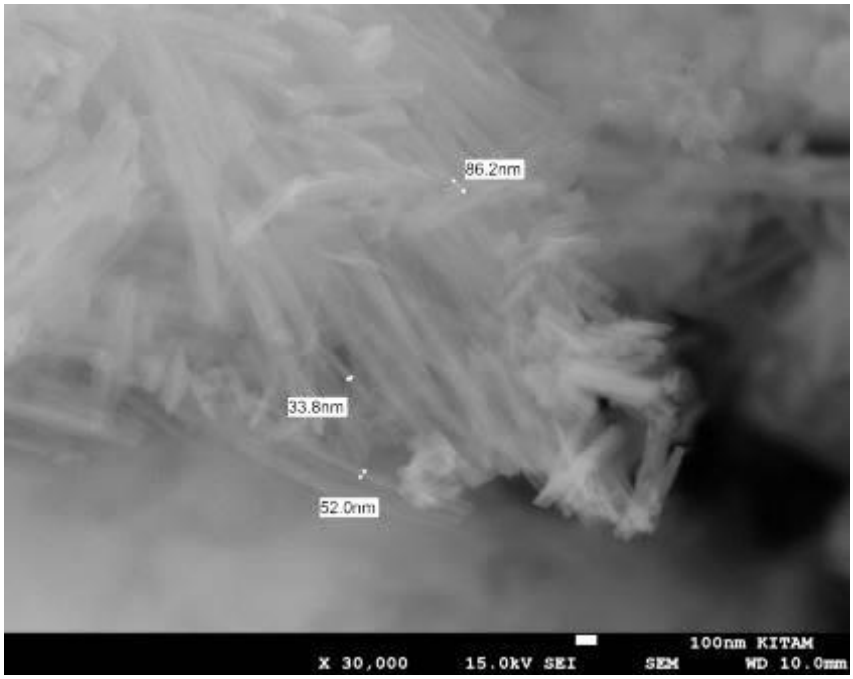

Fig. 4 SEM images of Mg@BTC

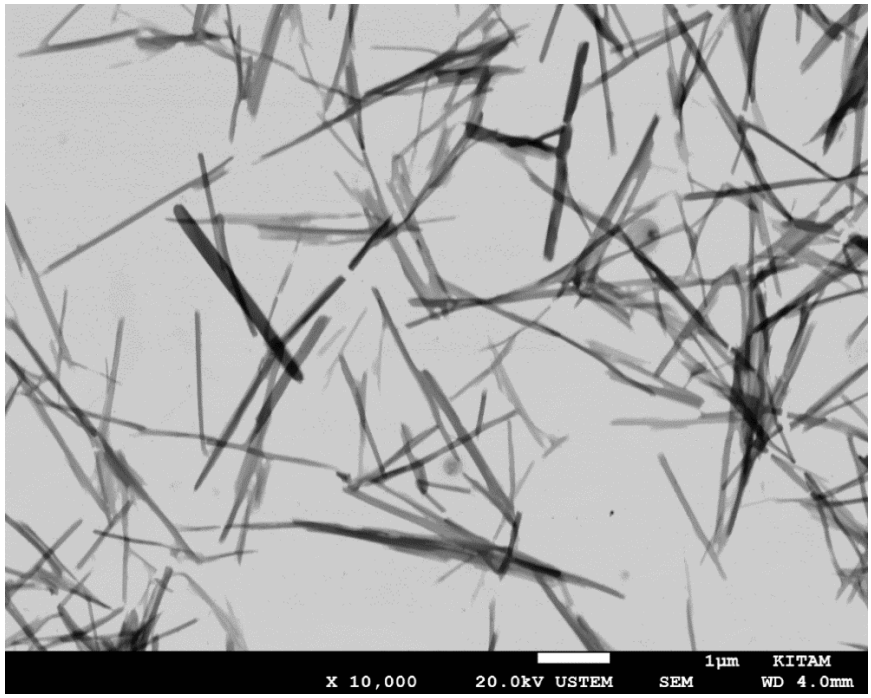

Fig. 5.- SEM images of Mg@BTC

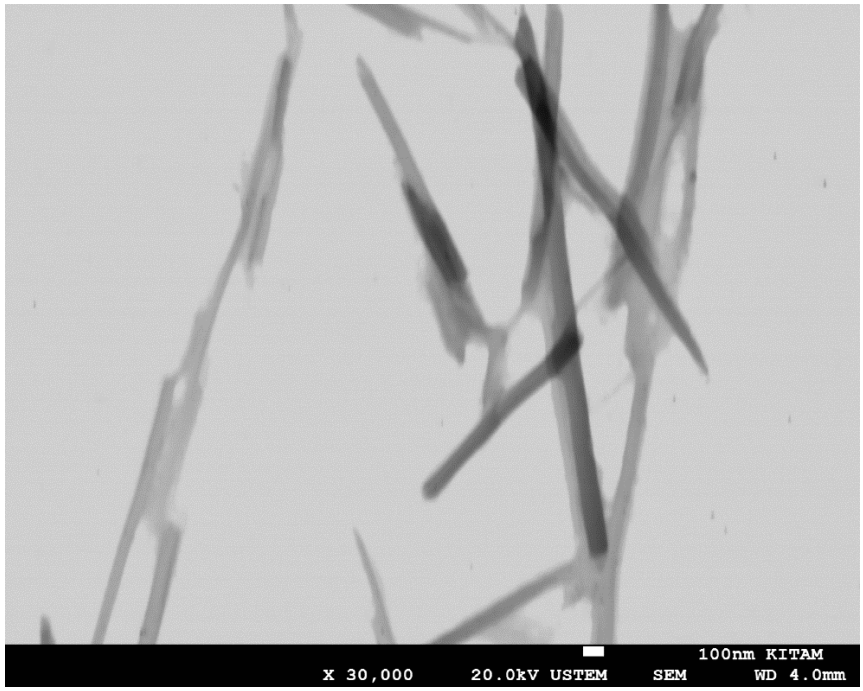

Fig. 6 SEM images of Mg@BTC.

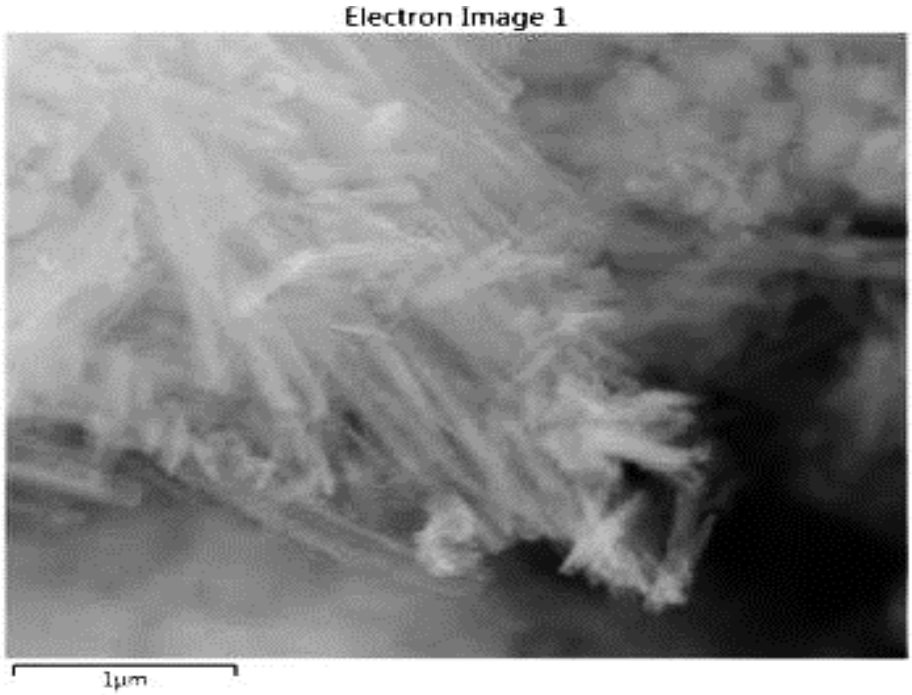

Fig. 7 SEM images of Mg@BTC.

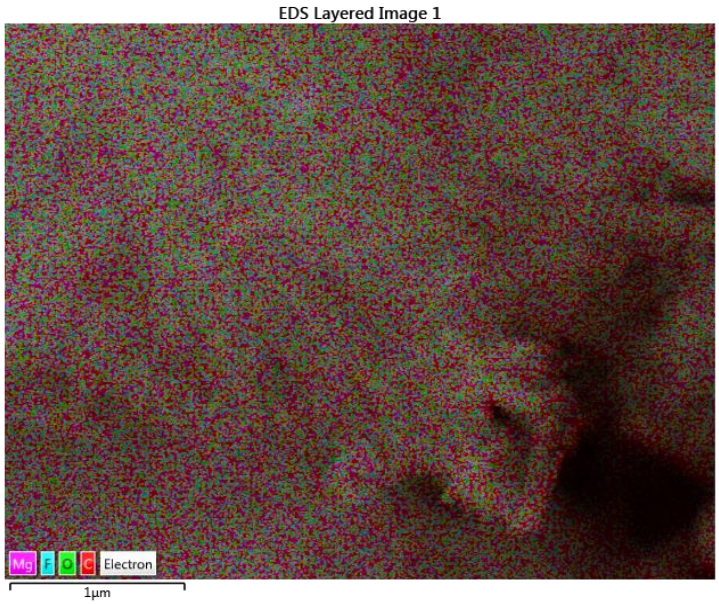

Fig. 8 EDS images of Mg@BTC.

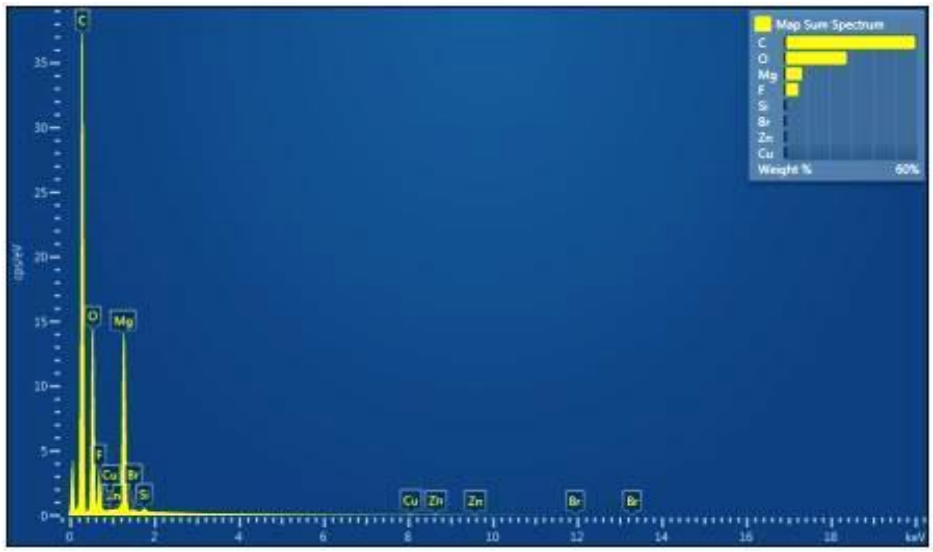

Fig. 9 EDS images of Mg@BTC.

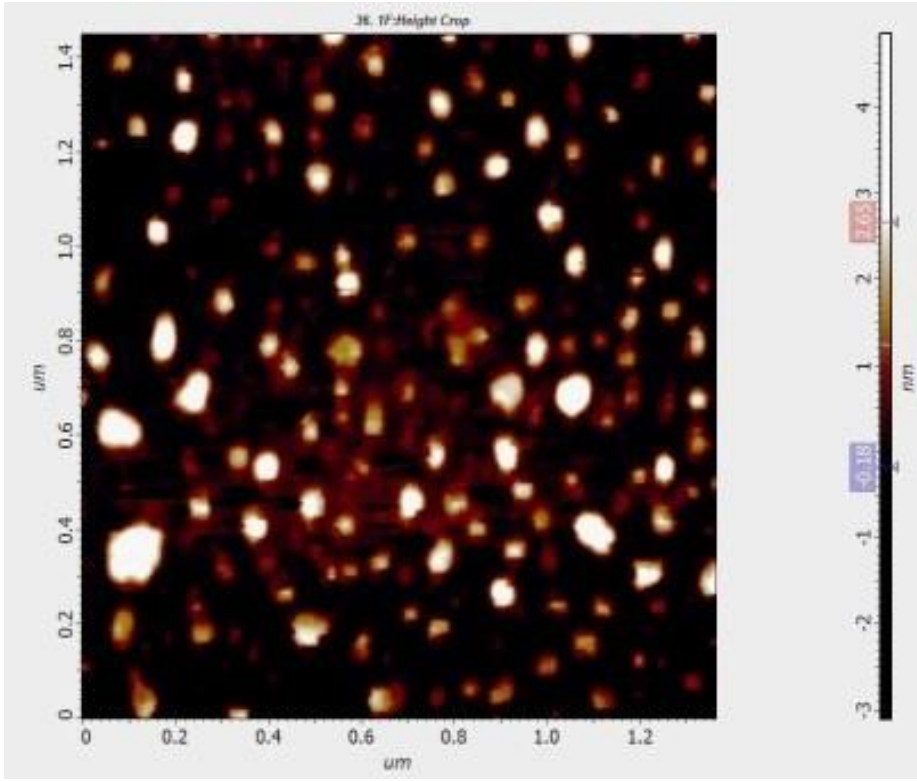

Fig. 10 AFM images of nano-sized Mg@BTC.

AFM images of nano-sized Mg@BTC are shown in Fig. 10. Based on AFM tapping mode images, Mg@BTC nanoparticles are filamentous-spherical in shape with homogeneous and regular distribution, and their sizes range from 30 to 100 nm.

3.1. Loading and release of ibuprofen into Mg@BTC

Concentration of loaded and released ibuprofen were calculated by the absorbance data obtained from UV-Vis spectroscopy. The UV-Vis spectra of ibuprofen in n-hexane is shown Fig. 11. The maximum wavelength at 220 nm was used for determining the concentration of loaded ibuprofen in the structure. The normal healthy body temperature 36 ± 0.5 °C and high body temperature 40 ± 0.5 °C were chosen for detected release behavior of ibu@[Mg@BTC].

The ibuprofen is loaded to the Mg@BTC 1:1 ratio with the amount of 99.8%. The PBS at the physiological pH was used for the *in vitro* drug release study. Maximum wavelength observed at the 228 nm is shown in Fig. 12. Ibuprofen loaded Mg@BTC showed a slow release over 100 h at 36 ± 0.5 °C. After 100 hours, the release ratio yields 36 % as shown in Fig. 13 and Fig. 14. As shown in Fig. 13, loaded ratio have slow release profile as compared with pure release and better holding capacity. The ibuprofen was loaded to the Mg@BTC 1:1 ratio with the amount of 112,5 mg was tested at 40 ± 0.5 °C. System showed a rapid release after 100 hours, the release ratio yield 72.29 % shown in Fig. 15 and Fig. 16.

These data indicate that Mg@BTC is effective nanocarrier and possess the slow released of ibuprofen. Drug could stay in the blood circulation very long time with slow release at 36 ± 0.5 °C. Thus, it could effect on the disease efficiently.

System showed a rapid release after 100 hours at 40 ± 0.5 °C. Which may be related to solubility of ibuprofen in aqueous solvents. Entropy, enthalpy, and Gibbs energy of the aqueous environment can be affected the solubility of ibuprofen at different temperature conditions. As was known, the solubility of ibuprofen are related to aqueous media [34]. Our results showed that ibuprofen possess rapid and control release under heat stoke conditions.

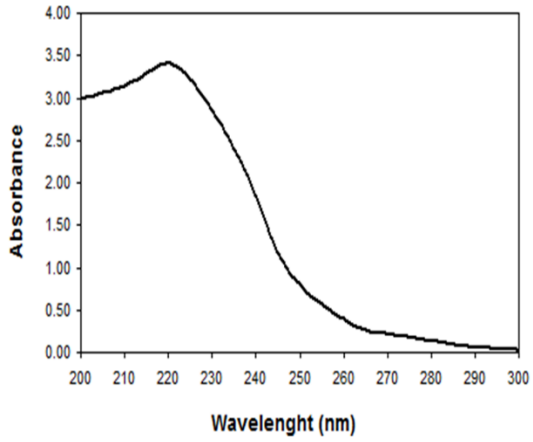

Fig. 11 UV-Vis spectra of ibuprofen in n-hexane.

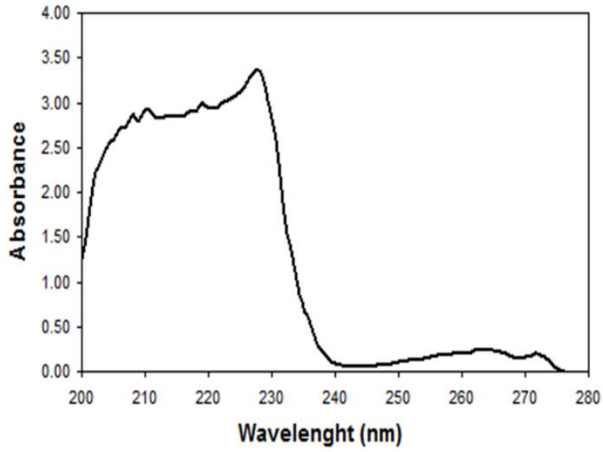

Fig. 12 UV-Vis spectra of ibuprofen in PBS and tween 20.

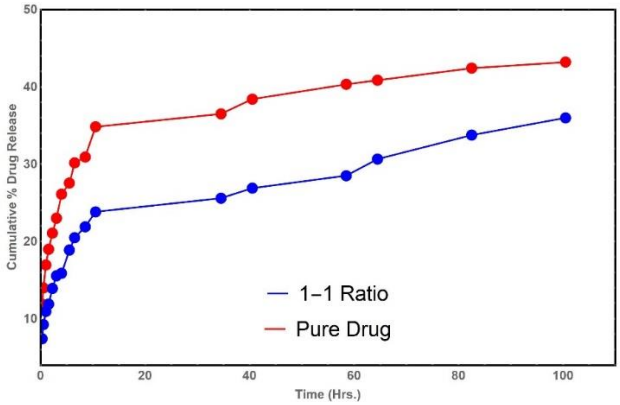

Fig. 13 Comparison of the release profiles.

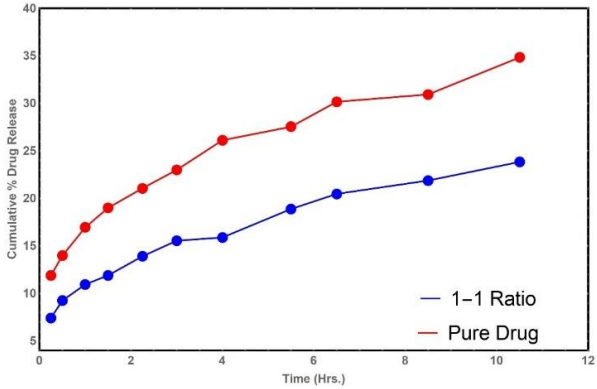

Fig. 14 Comparison of release profiles for short term.

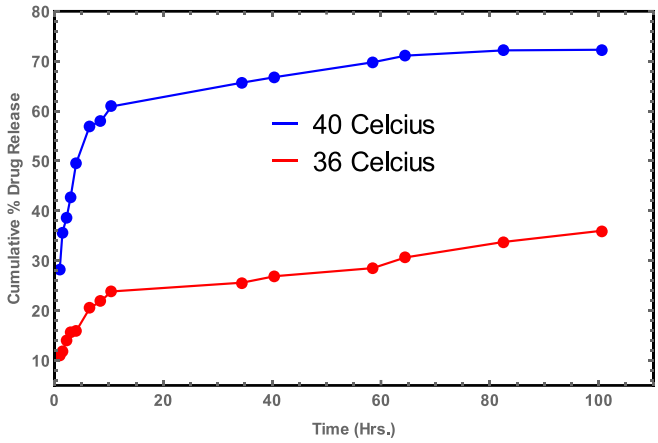

Fig. 15 Comparison of 1:1 ratio loaded drug release for 36 and 40 Celsius.

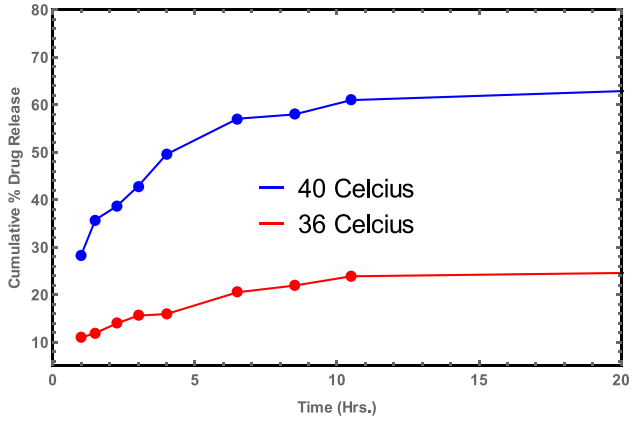

Fig. 16 Comparison of 1:1 ratio loaded drug release for 36 and 40 Celsius for short term.

4. Modeling

Mathematical modeling is essential for the comparison of the experimental results [25-27, 35-44]. They give us both graphical interference which gives us to chance for the prediction and numerical comparison to estimate the strength of the models. It is also obvious that graphical profile is the best way to generate comments on the dynamics of the system.

For the experiment described above, five mathematical models used. First two models are Zero Order Model and First Order Model from the reaction kinetics of the chemistry because these models represent the most basic release profile of the drug and from the nature of the generated equations, they can applied to release system easily. For the third model, it is decided to use Higuchi Model [1], because the Higuchi Model is the most famous mathematical representation of the drug release profile. And both its pure form and its modified form are used extensively to describe to drug release profile [2-4]. Also Peppas [27] and Hixon [28] models are added to the studies for their strong representations and usage frequency in the field. Solutions of these five models are respectively as;

$$C_t = C_0 \pm K_0 t \quad (1)$$

$$\log(C_t) = \log(C_0) - \frac{K_1 t}{2.303} \quad (2)$$

$$Q = K_2\sqrt{t} \quad (3)$$

$$Q = K_3 t^n \quad (4)$$

$$W_0^{1/3} - W_t^{1/3} = K_4 t \quad (5)$$

Where C_t is the amount of drug released at time t (and percent of drug remaining for the first order model), C_0 is the initial concentration of drug at time $t = 0$, K_0 is the zero-order rate constant, K_1 is the first order rate equation expressed in time^{-1} or per hour, Q is the cumulative amount of drug released in time t per unit area (and fraction of drug released at time t for Peppas model), K_2 is the Higuchi dissolution constant, K_3 is the Peppas release rate constant, W_0 is the amount of drug remaining at time t, W_t is the remaining amount of drug, K_4 is the Hixon constant describing surface volume relaxation.

For the fitting procedure of the models into the experimental data shouldn2t ignored for the model functions dependence. Otherwise fits are going to yield false results. For the Zero Order model it does not needed to make any change data matrix for the function is simple and the function varies with time only. For the First Order Model one should observe logarithmic percentage of the remaining drug because of the equation. So, the data matrix should be converted into logarithmic axes. For the Higuchi Model, drug release is pure function, but the time is increasing with the power of 1/2. So, the time part of the data matrix should be converted into the SQRT. Same kind of arrangements has been performed for other models as well. This is the only way to for generating meaningful results.

As it is seen from the graphs of the drug release profiles (Fig. 17, Fig. 18, Fig. 19, Fig. 20, Fig. 21), fit results are expressed according to their proper axes'. According to generated fit functions, the parameters of the functions are shown in Table 1

Table 1. The parameters of the fitted functions. Where C is the amount of drug released at time t (and percent of drug remaining for the first order model, K is the rate constant and n is the empirical parameter respectively.

Model	Parameters		
	C	K	n
Zero Order	14.65350	0.24091	-
First Order	85.14300	0.00316	-
Higuchi	-	11.24320	-
Peppas	-	11.97880	0.48056
Hixon	-	0.00826	-

In consideration to the derived parameters and fit strength table (Table 1), Peppas Model might be chosen for the best fit results and the better holding capacity to generate a predictive function as,

$$Q = 11.97880t^{0.48056} \quad (6)$$

which gives the 100% release after about 3.5 Days (82.74 hours). The reason of this surprising result comes from the difference between long and short term prediction. For the short time prediction, one may observe regular release up to 9 hours (Fig. 16) because the sink acts like a perfect sink and keeps the diffusion continuous state which is reasonable for the theoretical modeling studies, but it doesn't represent the experimental conditions appropriate way. After 9 hours, it is seen another release order which can be called long term release because according to experimental conditions the sink does not act like a perfect sink anymore. For the proper representation of the long term release this difference should not be ignored.

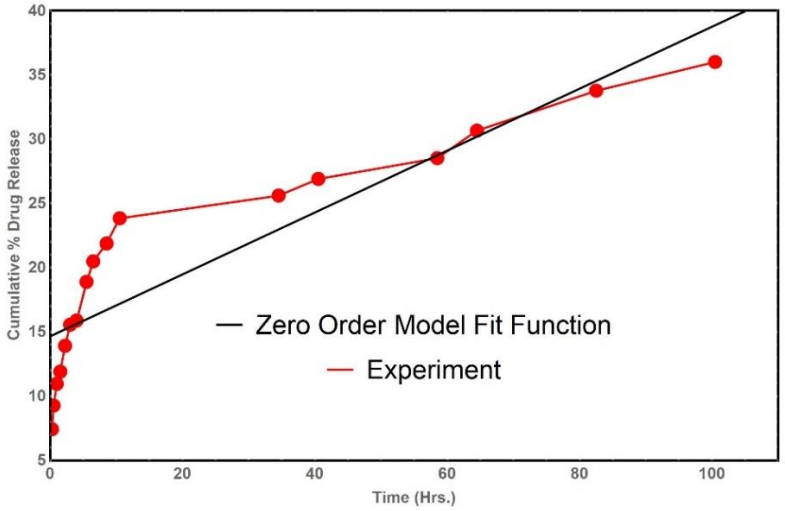

Fig. 17 1:1 Ratio release profile with Zero Order Model fit.

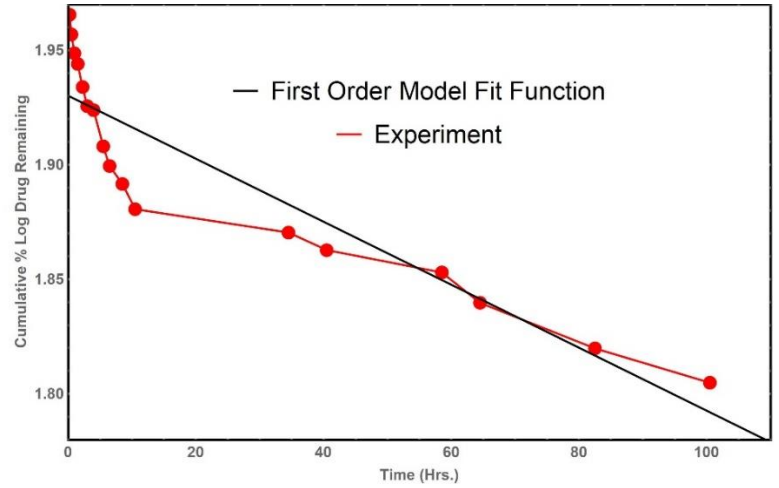

Fig. 18 1:1 Ratio release profile with First Order Model fit.

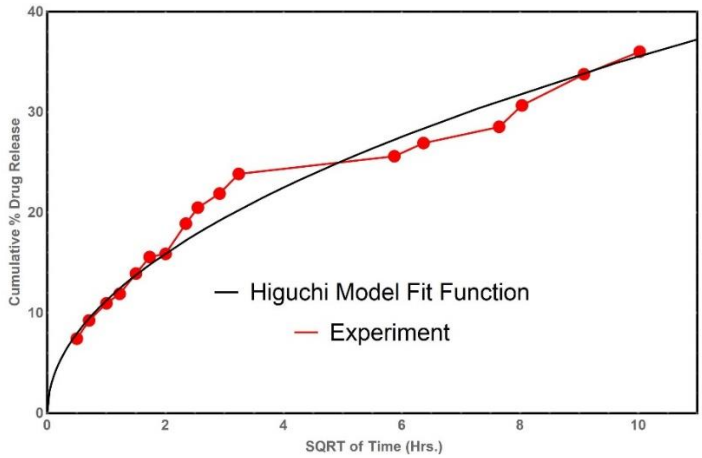

Fig. 19 1:1 Ratio release profile with Higuchi Model fit.

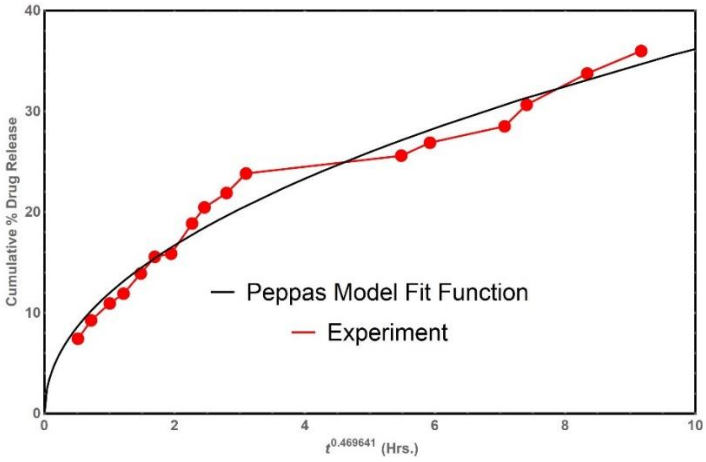

Fig. 20 1:1 Ratio release profile with Peppas Model fit.

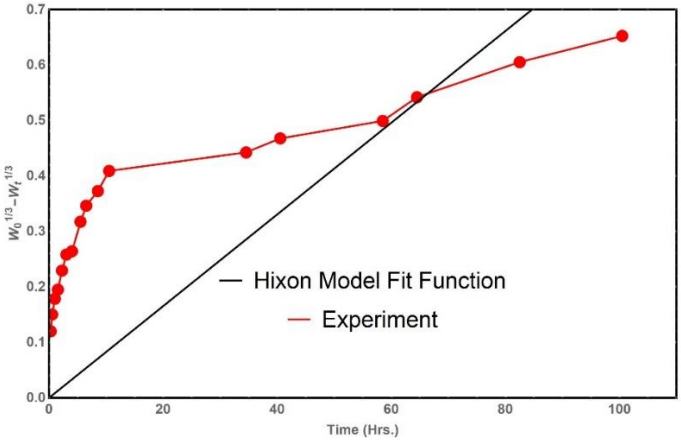

Fig. 21 1:1 Ratio release profile with Hixon Model fit.

Besides, for the comparison of the strength of the models Watson's U-Squared Method is used for the convenience of the data set. Which yields to two parameters as *statistic* and *P-Value*. For a strong model statistic should close to 0 and P-Value should close to 1. Statistic equals zero and P-Value equals 1 is mean perfect fit [29]. According to Watson's U-Squared test results, model parameters are shown in Table 2.

Table 2. Comparison of the fit results of the models according to Watson's U-Squared Method.

Model	Statistic	P-Value
Zero Order Model	0.125204	0.168768
First Order Model	0.125204	0.168768
Higuchi Model	0.038901	0.858828
Peppas Model	0.031981	0.929518
Hixon Model	0.371082	0.001180

According to the results it seems that it is needed to long hours to 100 % of pure drug release for experiment described above which is not make sense. The reason of the unexpected result is the difference between long- and short-term prediction. Short term predictions are only valid for sink conditions which the concentration is always zero. This phenomenon is also eligible for drug loaded nanocarriers.

For the thermodynamic analysis, the experimental results are shown in Fig. 24 and Fig. 25

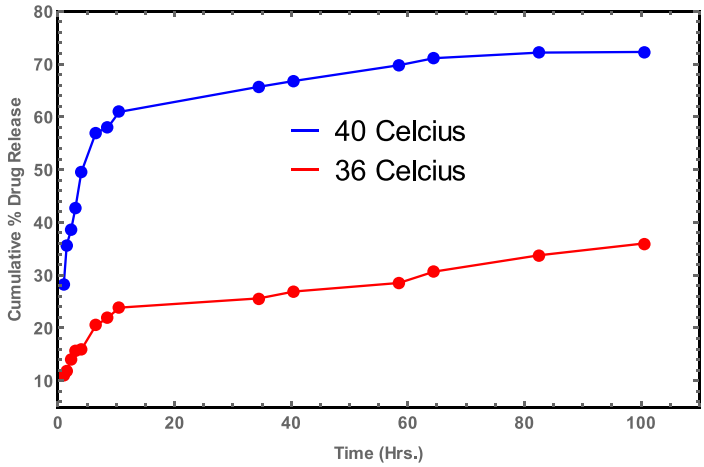

Fig. 22 Drug release profiles for 36 and 40 Celsius.

It is expected that faster release for higher temperature obviously. For finding activation energy, constant K is needed. In this study it is chosen Higuchi model (Eqn. 3) for evaluating that constant. Fitting results are shown in Table 3.

Table 3. K parameters for different temperatures

T (Kelvin)	K (hours^{-1})
309	4.18826
313	9.82826

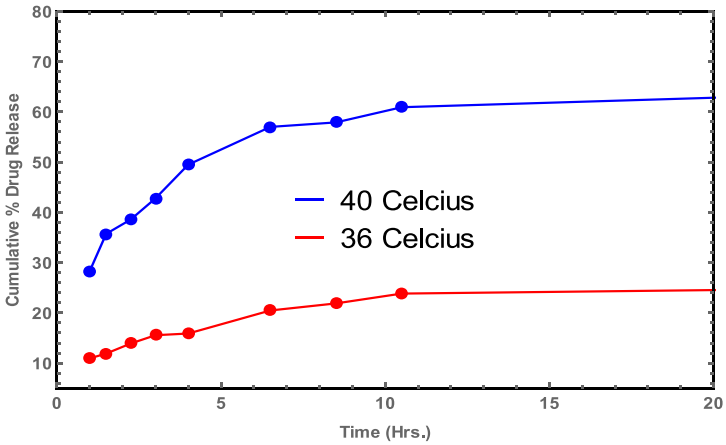

Fig. 23 Drug release profile for 36 and 40 Celsius up to 20 hours.

Arrhenius Equation [30] is used for evaluating activation energy.

$$K = Ae^{E_a/RT} \tag{7}$$

Where E_a is the activation energy $(kj.mol^{-1})$, R is the universal gas constant $(8314\ j/mol.K)$, T is the temperature (Kelvin). K is the reaction constant. Converting the Eqn. (7) into the $y = mx + n$ formation to get activation energy by slope, Fig. 24, it is found $E_a = 171636\ j/mol$.

$$\ln(k) = -\frac{E_a}{R}\left(\frac{1}{T}\right) + \ln(A) \tag{8}$$

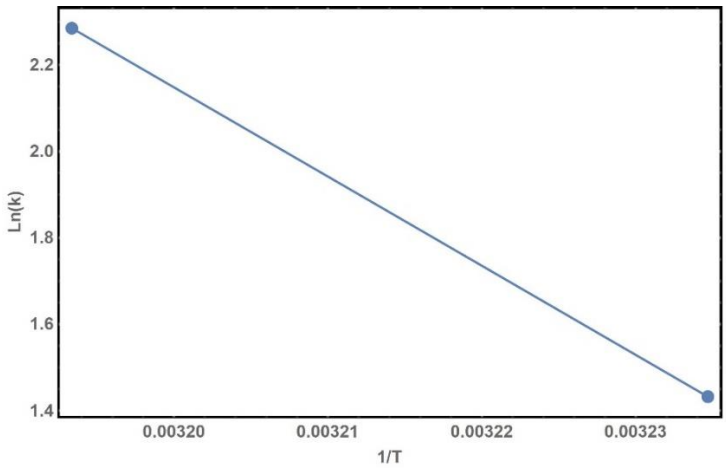

Fig. 24 Arrhenius slope.

Also, the Erying equation is used to get a thermodynamic parameters of the system [30].

$$ln\left(\frac{K}{T}\right) = \left[ln\left(\frac{K_b}{h}\right) + \frac{\Delta S}{R_g}\right] - \frac{\Delta H}{R_g} \times \frac{1}{T} \quad (9)$$

Where, K_b is the Boltzmann constant, h is the Plank constant, R_g is the universal gas constant, K is the reaction constant and T is the temperature (Kelvin). Converting the Eqn. (9) into $y = mx + n$ formation to get thermodynamic parameters by slope, Fig. 25, enthalpy is found $\Delta H = 169049\ j/mol$, and entropy is found $\Delta S = 313.514\ j/kg.K$

$$ln\left(\frac{K}{T}\right) = -\frac{\Delta H}{R} \times \frac{1}{T}\left[ln\left(\frac{K_b}{h}\right) + \frac{\Delta S}{R}\right] \quad (10)$$

Gibbs free energy is found by the Eqn. (11) for both temperatures [30] Table 4. Also, behavior of the system can observed by the Fig. 26 and Fig. 27

$$\Delta G = \Delta H - T \times \Delta S \quad (11)$$

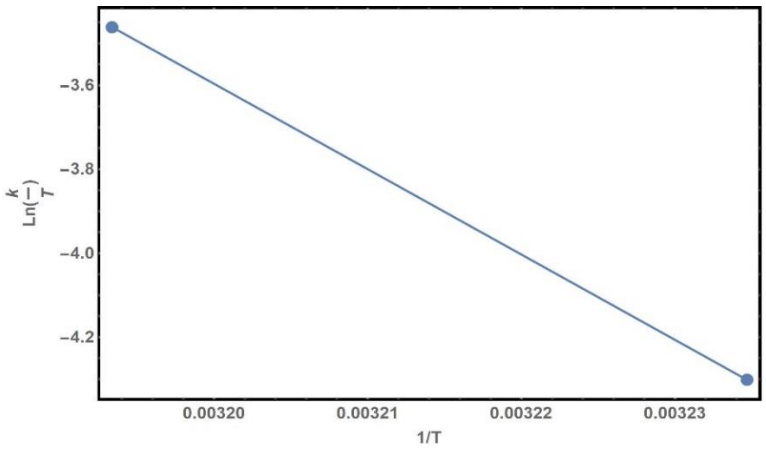

Fig. 25 ΔH Slope.

Table 4. Gibbs free energy values and reaction constants for different temperatures.

T (Kelvin)	$K\ (s^{-1})$	$\Delta G\ (j/mol)$
309	4.18826	72.1264
313	9.82826	70.8724

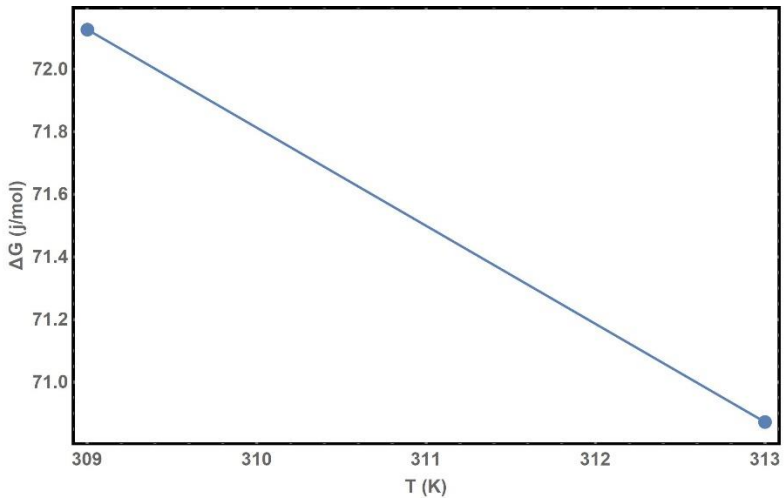

Fig. 26 Free energy change for different temperatures.

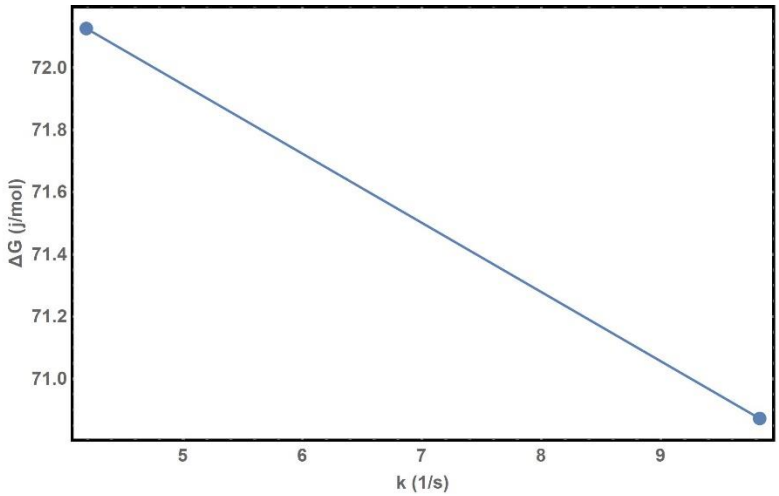

Fig. 27 Free energy change for different reaction constants.

5. Conclusions

In this study, nanosized Mg@BTC, synthesized by electrochemical method was used as a nanocarrier for ibuprofen first time. The ibuprofen was loaded to the Mg@BTC successfully. After long term release, the obtained release ratio was 36 % for 1:1. Mg@BTC could be afforded as a carrier for the slow-released of drug. Releasing of drug concentration for a specific period of time can be achieved by the Mg@BTC. Thus, it could effect on the disease efficiently. Besides, side effects can be eliminated in the bloodstream with the slow release.

Also, the release profile of the Mg@BTC is tested in the frame of mathematical models to get observation and prediction of the release patterns. Data sets are arranged for model suitable form thanks to the software. Five popular model functions are fitted to the release profiles. Watson's U-Squared Method is used to test the fit strength of the models.

According to the fit results for release profile are demonstrated that Peppas Model is the strongest one and predicted approximately 3.5 days of fully release. The short term dissolution profile of drug is different than the long term profile for that reason the used models have a limitation for the prediction of long term drug release pattern. Also, in thermodynamic studies, Fig. 26 showed that the increasing temperature results the free energy decrease, which means the loss of stability and holding capacity of the system is decreased. So, in further studies the temperature dependence should not be ignored.

The theoretical predictions have been foreseeing the better experiment conditions by avoiding waste of time and work power. In future studies, increasing the drug holding capacity will be studied thanks to the model fit results.

Acknowledgements

This study was completed as a part of BAP research project founded by the University of Ondokuz Mayıs (Project Number: PYO.FEN.1901.18.008).

References

[1] Gangu KK., et al. A review on contemporary Metal-Organic Framework materials. Inorganica Chimica Acta, 2016; 446:61-74. https://doi.org/10.1016/j.ica.2016.02.062
[2] Amir Reza Abbasi MR. Influence of the ultrasound-assisted synthesis of Cu-BTC metal-organic frameworks nanoparticles on uptake and release properties of rifampicin. Journal of Molecular Structure 2017; 36e42:1131.
[3] Lestari WW., et al. Green and facile synthesis of MOF and nano MOF containing zinc(II) and benzen 1,3,5-tri carboxylate and its study in ibuprofen slow-release. Materials Chemistry and Physics, 2018; 204:141-146. https://doi.org/10.1016/j.matchemphys.2017.10.034
[4] Alizadeh S, Nematollahi D. Electrochemically Assisted Self-Assembly Technique for the Fabrication of Mesoporous Metal-Organic Framework Thin Films: Composition of 3D Hexagonally Packed Crystals with 2D Honeycomb-like Mesopores. J Am Chem Soc, 2017; 139:13 4753-4761. https://doi.org/10.1021/jacs.6b12564
[5] Alinaghi Langari AA., et al. Efficient extraction of aromatic amines in the air by the needle trap device packed with the zirconium based metal-organic framework sorbent. RSC Advances, 2020; 10:23 13562-13572. https://doi.org/10.1039/D0RA00687D
[6] Firoozichahak A., et al. UIO-66-NH2 Packed Needle Trap for Accurate and Reliable Sampling and Analysis of the Halogenated Volatile Organic Compounds in Air. International Journal of Environmental Analytical Chemistry, 2019; 1-18. https://doi.org/10.1080/03067319.2019.1664497
[7] Firoozichahak A., et al. Development of a needle trap device packed with titanium-based metal-organic framework sorbent for extraction of phenolic derivatives in air. J Sep Sci, 2020; 43:5 1011-1018. https://doi.org/10.1002/jssc.201900938
[8] Pirmohammadi Z., et al. Determination of urinary methylhippuric acids using MIL-53-NH2 (Al) metal-organic framework in microextraction by packed sorbent followed by HPLC-UV analysis. Biomed Chromatogr, 2020; 34:1 e4725. https://doi.org/10.1002/bmc.4725
[9] Saedi N., et al. A needle trap device packed with MIL-100(Fe) metal organic frameworks for efficient headspace sampling and analysis of urinary BTEXs. Biomed Chromatogr, 2020; 34:4 e4800. https://doi.org/10.1002/bmc.4800
[10] Soury S., et al. Development of a needle trap device packed with zinc based metal-organic framework sorbent for the sampling and analysis of polycyclic aromatic hydrocarbons in the air. Microchemical Journal, 2019; 148:346-354. https://doi.org/10.1016/j.microc.2019.05.019
[11] Zhou JM,Shi W, Li HM, Li H, Cheng P. Phys. Chem. C, 2014; 118 416. https://doi.org/10.1021/jp4097502

[12] Yao Q., et al. Series of Highly Stable Isoreticular Lanthanide Metal-Organic Frameworks with Expanding Pore Size and Tunable Luminescent Properties. Chemistry of Materials, 2015; 27:15 5332-5339. https://doi.org/10.1021/acs.chemmater.5b01711
[13] K. Jihoon YS, Deok J, Seung YK. Microporous Mesoporous Mater, 2015; 202 8.
[14] Hu ZJ, Jian Z, Xiu FY, Xiao PS, Ai HY. Inorg. Chem. Commun, 2015; 54 54.
[15] Rao CNR., et al. Hybrid inorganic-organic materials: a new family in condensed matter physics (vol 20, art no 083202, 2006). Journal of Physics-Condensed Matter, 2008; 20:15. https://doi.org/10.1088/0953-8984/20/8/083202
[16] Yao Q, Gómez AB, Su J, Pascanu V, Yun Y, Zheng H, Chen H, Liu L, Abdelhamid HN, Martín-Matute B, Zou X. Chem. Mater, 2015; 27 5332. https://doi.org/10.1021/acs.chemmater.5b01711
[17] Blundell SJ, Pratt FL. Organic and molecular magnets. Journal of Physics-Condensed Matter, 2004; 16:24 R771-R828. https://doi.org/10.1088/0953-8984/16/24/R03
[18] Sheldon RA, Arends IWCE, Hanefeld U. Green Chemistry and Catalysis. Wiley-VCH, 2007. https://doi.org/10.1002/9783527611003
[19] Lucena FRS, de Araújo LCC, Rodrigues MD, da Silva TG, Pereira VRA, Militão GCG, Fontes DAF, Rolim-Neto PJ, da Silva FF, Nascimento SC. Induction of cancer cell death by apoptosis and slow release of 5-fluoracil from metal-organic frameworks Cu-BTC. Biomedicine & Pharmacotherapy. Silene C. Nascimento, 2013; 67 707-713. https://doi.org/10.1016/j.biopha.2013.06.003
[20] Lazaro IA, Forgan RS. Application of zirconium MOFs in drug delivery and biomedicine. Coordination Chemistry Reviews, 2019; 380:230-259. https://doi.org/10.1016/j.ccr.2018.09.009
[21] Silva EDV., et al. Solvent-free synthesis of acetylated cashew gum for oral delivery system of insulin. Carbohydrate Polymers, 2019; 207:601-608. https://doi.org/10.1016/j.carbpol.2018.11.071
[22] Vasconcelos IB, Wanderley KA, Rodrigues NM, da Costa Jr. NB, Freire RO, Junior SA. Host-guest interaction of ZnBDC-MOF þ doxorubicin: A theoretical and experimental study. Journal of Molecular Structure, 2017; 1131 36e42. https://doi.org/10.1016/j.molstruc.2016.11.034
[23] Bushra R, Aslam N. Oman Med. J., 2010; 25 (3) 155e1661. https://doi.org/10.5001/omj.2010.49
[24] Moss Jr WM, Bendel Lp, Et Al. A multicenter, randomized, double-blind placebo-controlled, single dose trial of the safety and efficacy of intravenous ibuprofen for treatment of pain in pediatric patients undergoing tonsillectomy. Paediatr Anaesth, 2014; 9:24 483. https://doi.org/10.1111/pan.12381
[25] Gouda R. Baishya H, Qing Z. Application of Mathematical Models in Drug release Kinetics of Carbidopa and Levadopa ER Taablets. Journal of Developing Drugs, 2017; 6:2.
[26] Higuchi T., et al., Pharmaceutical analysis, Interscience Publishers, New York,, 1961.
[27] Ritger PL, Peppas NA. Transport of Penetrants in the Macromolecular Structure of Coals .7. Transport in Thin Coal Sections. Fuel, 1987; 66:10 1379-1388. https://doi.org/10.1016/0016-2361(87)90185-2
[28] Hixon AW, Crowell JH. Dependence of Reaction Velocity upon Surface and Agiation. Industrial and Engineering Chemistry, 1931; 923-931. https://doi.org/10.1021/ie50260a018
[29] Batschelet E. United States. Office of Naval Research., Statistical methods for the analysis of problems in animal orientation and certain biological rhythms, American Institute of Biological Sciences, Washington, 1965.
[30] Freire LMC., et al. Understanding Drug Release Data through Thermodynamic Analysis. Materials, 2017; 10:6. https://doi.org/10.3390/ma10060651

[31] Wang Z., et al. Self-Supported Catalysts. Chemical Reviews, 2009; 109:2 322-359. https://doi.org/10.1021/cr800406u
[32] Gaffney JS, Marley NA, Jones DE. Fourier Transform Infrared (FTIR) Spectroscopy. Characterization of Materials, 2012. https://doi.org/10.1002/0471266965.com107.pub2
[33] Bella F., et al. Light cured networks containing metal organic frameworks as efficient and durable polymer electrolytes for dye-sensitized solar cells. Journal of Materials Chemistry A, 2013; 1:32 9033-9036. https://doi.org/10.1039/c3ta12135f
[34] Garzon LC, Martinez F. Temperature Dependence of Solubility for Ibuprofen in Some Organic and Aqueous Solvents. Journal of Solution Chemistry, 2004; 33:11 1379-1395. https://doi.org/10.1007/s10953-004-1051-2
[35] Langer R, Peppas N. Chemical and Physical Structure of Polymers as Carriers for Controlled Release of Bioactive Agents - a Review. Journal of Macromolecular Science-Reviews in Macromolecular Chemistry and Physics, 1983; C23:1 61-126. https://doi.org/10.1080/07366578308079439
[36] Plackett RL. Pearson,Karl and the Chi-Squared Test. International Statistical Review, 1983; 51:1 59-72. https://doi.org/10.2307/1402731
[37] Ju RTC., et al. Drug-Release from Hydrophilic Matrices .1. New Scaling Laws for Predicting Polymer and Drug-Release Based on the Polymer Disentanglement Concentration and the Diffusion Layer. Journal of Pharmaceutical Sciences, 1995; 84:12 1455-1463. https://doi.org/10.1002/jps.2600841213
[38] Fick A. On Liquid Diffusion (Reprinted from the London, Edinburgh, and Dublin Philosophical Magazine and Journal of Science, Vol 10, Pg 30, 1855). Journal of Membrane Science, 1995; 100:1 33-38. https://doi.org/10.1080/14786445508641925
[39] Narasimhan B, Peppas NA. Molecular analysis of drug delivery systems controlled by dissolution of the polymer carrier. J Pharm Sci, 1997; 86:3 297-304. https://doi.org/10.1021/js960372z
[40] Langer MB. Drugs and the pressure to be perfect, Rosen Pub. Group, New York, 1998.
[41] Siepmann J., et al. A new model describing the swelling and drug release kinetics from hydroxypropyl methylcellulose tablets. Journal of Pharmaceutical Sciences, 1999; 88:1 65-72. https://doi.org/10.1021/js9802291
[42] Siepmann J., et al. HPMC-matrices for controlled drug delivery: A new model combining diffusion, swelling, and dissolution mechanisms and predicting the release kinetics. Pharmaceutical Research, 1999; 16:11 1748-1756.
[43] Siepmann J, Peppas NA. Modeling of drug release from delivery systems based on hydroxypropyl methylcellulose (HPMC). Advanced Drug Delivery Reviews, 2001; 48:2-3 139-157. https://doi.org/10.1016/S0169-409X(01)00112-0
[44] Grassi M., et al. Modeling of drug release from partially coated matrices made of a high viscosity HPMC. International Journal of Pharmaceutics, 2004; 276:1-2 107-114. https://doi.org/10.1016/j.ijpharm.2004.02.016